Correction of C-band radar observation for propagation effects based on the self-consistency principle

Ahoro Adachi[1], Takahisa Kobayashi[2,1] and Hiroshi Yamauchi[1]

[1]*Meteorological Research Institute, 1-1 Nagamine, Tsukuba 305-0052, Japan*
[2]*Central Research Institute of Electric Power Industry, 1646 Abiko, Abiko-city 270-1194, Japan*
(Dated: 18 July 2014)

1 Introduction

Many studies have proposed methods to estimate DSD parameters as a part of rain attenuation correction and/or rainfall rate estimation algorithms. The DSD parameters may provide information that is useful for exploring rain microphysics in clouds, which is one of the advantages of this type of method. The atenuation correction and DSD retrieval algorithms proposed in the present study are based on an autocalibration of Z_H using polarization redundancy introduced by Goddard et al. (1994), which is a variation of the calibration method by Gorgucci et al. (1992). Goddard et al. (1994) showed that for rain, K_{DP}/Z_H is a unique function of Z_{DR}, which is virtually independent of μ, and proposed that this self-consistency could be used to provide an automatic calibration of Z_H to within 0.5 dB for S-band (Illingworth 2004), where the path-integrated attenuation is negligible. For radars operating at higher frequency, Le Bouar et al. (2001) expressed concern over attenuation of Z_H and Z_{DR} when applying the autocalibration for C-band. On the other hand, Thurai and Hanado (2005) showed that this technique is available for C-band even in heavy rain if reference DSD data measured by 2DVD are provided to estimate attenuation effects. Moreover, Bringi et al. (2006) retrieved D_0 from C-band radar measurements and 2DVD reference data by using the consistency among the polarimetric measurements on which the autocalibration technique is based. This result suggests that the autocalibration can be used to retrieve DSD parameters if reliable corrections for attenuation are applicable. Thus, in this study, we propose a new algorithm to correct rain attenuation and estimate the three DSD parameters and rainfall rates for polarimetric radar at attenuation frequency by expanding the self-consistency principle among the polarimetric measurements. The proposed algorithm requires no external reference data such as 2DVD measurements for attenuation corrections because it retrieves co-polar and differential specific attenuations from the interrelation among the polarimetric measurements.

2 Description of polarimetric method to correct attenuations and retrieve DSD based on consistency theory

2.1 Autocalibration technique

This study develops an algorithm to correct attenuation and retrieve the three DSD parameters from polarimetric measurements by expanding an autocalibration of Z proposed by Goddard et al. (1994). They showed that K_{DP}/Z is a unique function of Z_{DR} for rain, as shown in Fig. 1, and proposed an automatic calibration technique of Z for S-band radar using this redundancy relation. The technique is as follows: For given values of μ and raindrop temperature, K_{DP} can be inferred from the observed values of Z_{DR} and Z at each gate along a ray from the consistency curve (Fig. 1), and the predicted K_{DP} at each gate can be summed to obtain the theoretical Φ_{DP}. The theoretical Φ_{DP} can be compared with the smoothed-observed Ψ_{DP} (i.e., the pseudo-observed ΦDP) and the value of Z scaled until the computed value agrees with the observed value (Illingworth 2004). Figure 1 shows that the consistency curve has low μ and temperature dependency for C-band, but it has slightly higher dependency for X-band.

Because this autocalibration technique does not take the attenuation effect into account, it is valid for S-band but limited for C-band to use with weak rain when the attenuation effect is negligibly small. Unfortunately, this technique is practically impossible for radars operating at X-band to use without attenuation corrections, as Gourley et al. (2009) pointed out. In the case of heavy rainfall, attenuation corrections should be applied in advance for measured Z_H and Z_{DR} to yield theoretical K_{DP} from the consistency curve for those radars. Thurai and Hanado (2005) and Bringi et al. (2006) used K_{DP} derived from the measured Ψ_{DP} to correct attenuations for Z_H and Z_{DR}. However, they needed 2DVD measurements to estimate a relation between K_{DP} and attenuations. Following their studies, we expand the consistency relationship, which governs the autocalibration, to include attenuation correction procedures that do not require any external reference DSD data and develop an automatic DSD parameter retrieval technique for radars at attenuating frequency with heavy rainfall.

aadachi @mri-jma.go.jp

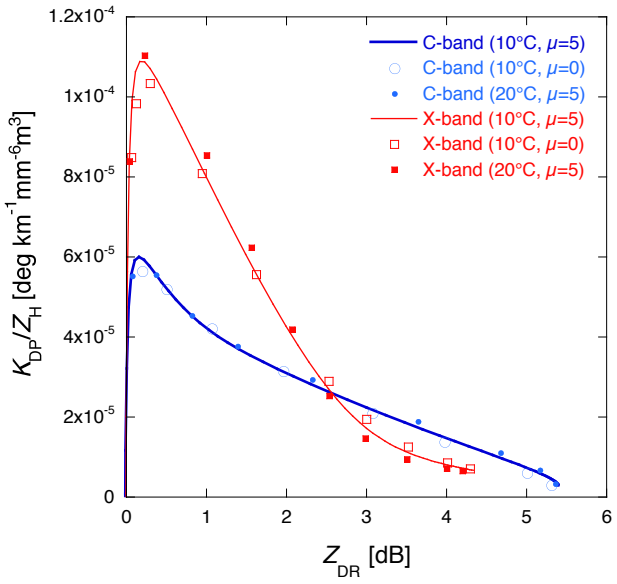

Figure 1. Relationship between two-way specific differential phase per unit linear horizontal reflectivity as a function of differential reflectivity at raindrop temperatures of 10 °C and 20 °C at C-band (5.370 GHz) and X-band (9.375 GHz) with shape parameters of 0 and 5 for a modified gamma distribution with the axis ratio of Brandes et al. (2005).

2.2 Expansion of consistency relationship and attenuation correction

The attenuation correction algorithm used in the present study assumes that the raindrop temperature and operating frequency are given and that all polarimetric variables including attenuations are determined by the DSD, which is represented by the modified gamma distribution. Also, no ice hydrometeors (such as hail and/or graupel) are assumed to be included in the range profile. These issues are addressed in later sections. The theoretical variations of the functions of A_H/Z_H and A_{DP}/Z_H with Z_{DR} at raindrop temperatures of 0 and 20°C with shape parameters of 0 and 5 are shown in Figs. 2a and 2b, respectively. In the derivation of the new consistency curves, the minimum diameter (D_{min}) of 0.1 mm and the maximum diameter (D_{max}) of 8 mm are used.

Figure 2 indicates that the consistency curve of A_H/Z_H has low temperature and shape-parameter dependencies, especially for C-band, as is the case for K_{DP}/Z_H. However, this figure also shows that the consistency curve of A_{DP}/Z_H has slightly larger dependencies not only on temperature but also on shape parameter, especially for X-band. These small dependencies on both temperature and shape parameter could make large differences in the retrieval of rainfall rate, particularly in heavy rainfall, because the attenuation effects are defined as path integrals of the co-polar and differential specific attenuations given by

$$Z_H^{obs}(r) = Z_H^{true}(r) - 2\int_{r_1}^{r} A_H(s)ds - C_H \tag{1}$$

and

$$Z_{DR}^{obs}(r) = Z_{DR}^{true}(r) - 2\int_{r_1}^{r} A_{DP}(s)ds - C_{DP}, \tag{2}$$

where Z_H^{true} (dBZ) and Z_{DR}^{true} (dB) represent true reflectivity and differential reflectivity after attenuation correction at a range of r, respectively, r_1 is the distance of the first range resolution volume, and C_H and C_{DP} are the correction terms for the reflectivity and differential reflectivity profiles, respectively.

We have opted for a simple gate-to-gate attenuation correction scheme as opposed to the more complicated techniques used, for example, by Testud et al. (2000) or Yoshikawa et al. (2014). In the proposed algorithm, the true reflectivity and differential reflectivity at range rn can be obtained by recurrence formulas derived from Eqs. (1) and (2) as

$$Z_H^{true}(r_n) = Z_H^{obs}(r_n) + 2\sum_{k=1}^{n} A_H\left(Z_H^{true}(r_{k-1}), Z_{DR}^{true}(r_{k-1})\right)\delta s + C_H, \tag{3}$$

$$Z_{DR}^{true}(r_n) = Z_{DR}^{obs}(r_n) + 2\sum_{k=1}^{n} A_{DP}\left(Z_H^{true}(r_{k-1}), Z_{DR}^{true}(r_{k-1})\right)\delta s + C_{DP}, \tag{4}$$

aadachi @mri-jma.go.jp

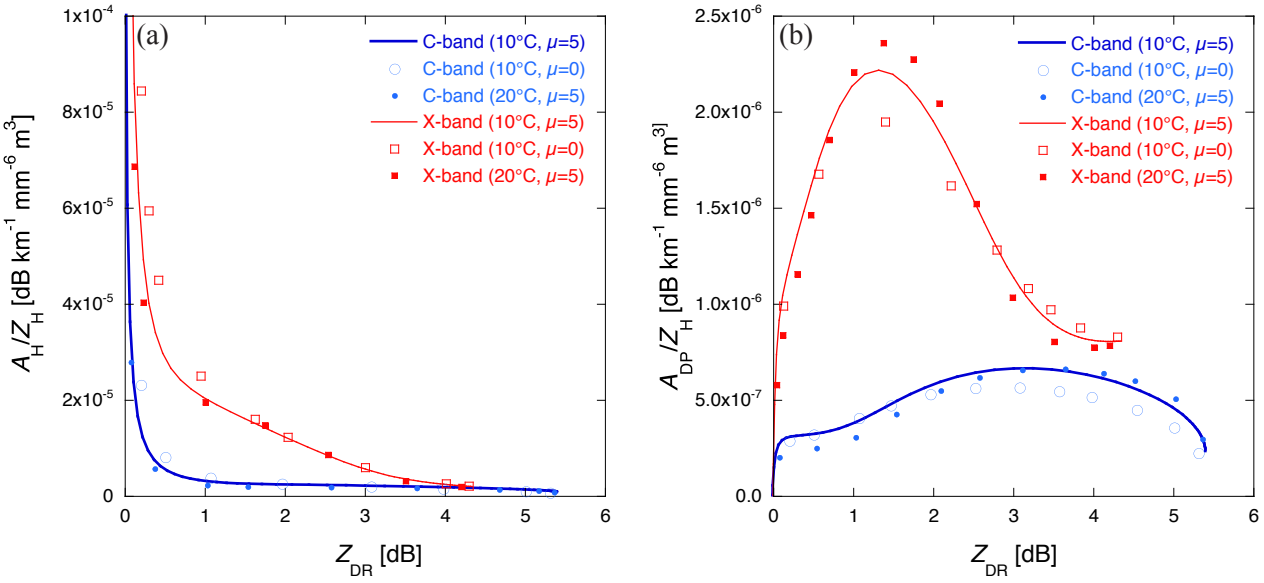

Figure 2. (a) Relationships of horizontal specific attenuation per unit linear horizontal reflectivity and (b) specific differential attenuation per unit linear horizontal reflectivity as a function of differential reflectivity at raindrop temperatures of 10 °C and 20 °C at C-band (5.370 GHz) and X-band (9.375 GHz) with shape parameters of 0 and 5 for a modified gamma distribution with the axis ratio of Brandes et al. (2005).

where r_n represents the distance of the nth range gate, δs (km) is the range resolution of the radar measurements and

$$Z_H^{true}(r_n) = Z_H^{obs}(r_n) + 2\sum_{k=1}^{n} A_H\left(Z_H^{true}(r_{k-1}), Z_{DR}^{true}(r_{k-1})\right)\delta s + C_H \quad (5)$$

Note that the co-polar and differential specific attenuations are inferred from true Z_H and Z_{DR} with the consistency curves in Figs. 2a and 2b, respectively. The bias (C_H) in the observed Z_H corrected with the proposed method is the sum of the radar constant calibration error and any excess attenuation from the radar to the first range resolution volume, including excess attenuation due to rain on the radome, as shown in Eq. (5) and as assumed in Bringi et al. (2006) and Thurai and Hanado (2005). Similarly, the term C_{DP} is the sum of relative bias error in Z_{DR} and excess differential attenuation. In the method used here, it is also assumed that the systematic bias in Z_{DR} measurements is negligible (by calibrating with vertical measurements in rain) and that excess differential attenuation can be neglected assuming that both the H and V signal powers are affected almost equally by rain on the radome, which is supported by the results of Gorgucci et al. (2013). Therefore, the value of C_{DP} is set to zero, as assumed in Bringi et al. (2006).

In the proposed method, Eqs. (3) and (4) are initially evaluated assuming C_H to be zero. Once values of the true Z_H and Z_{DR} so derived at each gate are obtained, they are used to predict the value of K_{DP} at that gate with the original consistency curves (Fig. 1). The theoretical Φ_{DP} can be derived from the predicted K_{DP}, and the values of measured Z are scaled by C_H in Eq. (3) so that the total phase change of the theoretical Φ_{DP} along the path agrees with that of the smoothed-observed Ψ_{DP}, as is done in the original autocalibration technique.

Since this method requires the total phase change of the smoothed-observed Ψ_{DP} at sufficiently large distance, it may not be available under extreme attenuation conditions in which signal is completely lost. Moreover, the attenuation correction procedure proposed in the present study is based on gate-by-gate recursive estimation through a relationship employing the measured Z_H and Z_{DR}. This approach is very sensitive to any bias on Z_H and Z_{DR} (e.g., hail, graupel, ground clutter, and partial beam blockage). Contamination from these biases may result in large errors in the retrievals of rain parameters with the proposed algorithm. However, contamination from these biases in a radial direction can be identified and discarded by this method because it produces a large error in the theoretical Φ_{DP} profile, and the theoretical Φ_{DP} diverges from the smoothed-observed Ψ_{DP} abruptly. Indeed, we observed theoretical Φ_{DP} deviated from the smoothed-observed Ψ_{DP} by more than 100° within a few gates behind ground clutters in the observations with an antenna elevation angle of 0.5°. Fortunately, all the theoretical Φ_{DP} profiles analyzed in this study fit the smoothed-observed Ψ_{DP} made at an elevation angle of 1.0°, which suggests that the observations were made in pure rain conditions.

aadachi @mri-jma.go.jp

2.3 Retrieval of the DSD parameters

The DSD parameters are derived from the attenuation-corrected Z_H and Z_{DR} obtained with the proposed method. A modified gamma distribution model suggested by Ulbrich (1983) has been used to characterize the natural variation of DSD, which is given by,

$$N(D) = N_0 D^{\mu} \exp\left(-\frac{3.67+\mu}{D_0}\right), \tag{6}$$

where D (mm) is the equivalent-volume spherical raindrop diameter, N_0 ($mm^{-1-\mu}$ m^{-3}) is the raindrop concentration and μ (unitless) and D_0 (mm) represent the shape parameter and median volume diameter of the distribution, respectively. Rainfall rate R (mm h-1) can be derived from DSD by

$$R = 0.6\pi \times 10^{-3} \int_0^{\infty} v(D) D^3 N(D)\, dD, \tag{7}$$

where $v(D)$ (m s^{-1}) is the raindrop terminal velocity. Dual polarimetric radar observables such as horizontal reflectivity Z_H (mm^6 m^{-3}), vertical reflectivity Z_V (mm^6 m^{-3}), and Z_{DR} (dB) can be also expressed in terms of raindrop size distribution as

$$Z_{H,V} = 10^{18} \times \frac{\lambda^4}{\pi^5 |K|^2} \int_{D_{\min}}^{D_{\max}} 4\pi \left|S_{hh,vv}(D)\right|^2 N(D)\, dD, \tag{8}$$

and

$$Z_{DR} = 10 \log\left(\frac{Z_H}{Z_V}\right), \tag{9}$$

where λ (m) is the wavelength, $S_{hh,vv}$ (m) are the backscattering co-polar components of the scattering amplitude matrix, D_{min} and D_{max} (mm) are the minimum and maximum drop diameters, respectively, and K is a constant defined as $K = (\varepsilon - 1)/(\varepsilon + 2)$, where ε is the complex dielectric constant of water estimated as a function of wavelength and temperature.

Horizontal reflectivity Z_H and vertical reflectivity Z_V can be expressed in terms of the raindrop concentration N_0 by substituting Eq. (6) for Eq. (8) as

$$Z_{H,V} = N_0 \times F_{H,V}(\mu, D_0), \tag{10}$$

where

$$F_{H,V}(\mu, D_0) = 10^{18} \times \frac{\lambda^4}{\pi^5 |K|^2} \int_{D_{\min}}^{D_{\max}} 4\pi \left|S_{hh,vv}(D)\right|^2 D^{\mu} \exp\left(-\frac{3.67+\mu}{D_0} D\right) dD. \tag{11}$$

By substituting (11) into (9), we derive the differential reflectivity, Z_{DR} as

$$Z_{DR} = 10 \log\left(\frac{N_0 \times F_H(\mu, D_0)}{N_0 \times F_V(\mu, D_0)}\right) \equiv G_{DR}(\mu, D_0). \tag{12}$$

The shape parameter is estimated by comparing the theoretical Φ_{DP} with the smoothed-observed Ψ_{DP} through a rain path in the radial direction so that the root-mean-square of the difference takes the minimum value. Once the shape parameter is determined, the equivalent volume diameter D_0 can be derived from the attenuation-corrected Z_{DR} at each range gate because Z_{DR} is independent of N_0 and is a function of D_0 and μ, as given by Eq. (12). Then, N_0 can be derived from the true Z_H with the retrieved D_0 and μ from Eq. (10), and rainfall rate can be obtained from the DSD through Eq. (7), once the raindrop terminal velocity is provided. In the present study, the drop terminal velocity proposed by Lhermitte (1990) was used in Eq. (7). For the details of the autocalibration and the DSD parameter retrieval, see Adachi et al (2013b).

3. MRI C-band polarimetric radar and retrieval of DSD parameters

In this section, we apply the proposed algorithm for actual C-band polarimetric radar data in order to demonstrate the high reliability of this method by comparing the retrieved data with measurements on the ground.

aadachi @mri-jma.go.jp

Table 1. Operating characteristics of the MRI C-band polarimetric radar.

Frequency	5370 MHz
Occupied band width	< 4.5 MHz
Peak power	3.5 kW (for each channel, simultaneous transmission)
Duty	20 % (Max)
Pulse length	1μs (range < 20 km) and 129 μs (≥ 20 km) for Elv. < 8°
	1μs (range < 7.5 km) and 47 μs (≥ 7.5 km) for Elv. ≥ 8°
Pulse compression	Linear FM chirp for long-pulse observations
Antenna diameter	Parabolic dish, Φ = 4 m
Antenna speed	4 rpm for Elv. <8° and 6 rpm for Elv. ≥ 8° (10 rpm Max.)
Signal minimum	< -110 dBm
Antenna gain (H and V)	> 42 dBi
Max cross-polar isolation	< -40 dB
Beam width	1.01°
Azimuth spacing	0.7°
Transmitter	GaAs Power FET
Number of linear sampling	20
Range Gate Spacing	150 m
PRF	624/780 Hz (Elv. < 8°) and 936/1170 Hz (Elv. ≥ 8°)
Observation parameters	ZH, ZV, ZDR, radial velocity, ρHV(0) and ΨDP

3.1 MRI C-band polarimetric radar

The Meteorological Research Institute (MRI) advanced C-band solid-state polarimetric radar (MACS-POL radar) is mounted on top of the MRI building in Tsukuba, Japan (Adachi et al. 2013a). The radar routinely collects a full suite of dual-polarization measurements, including the reflectivity factor (Z_H), differential reflectivity (Z_{DR}), differential propagation phase (Ψ_{DP}), and correlation coefficient at zero lag ($\rho_{HV}(0)$). This system employs two solid-state amplifier units to transmit horizontally and vertically polarized waves. The radar is operating in the simultaneous transmission and reception (STAR) mode for polarized signals, i.e., the system simultaneously transmits horizontal and vertical polarization states and obtains samples of both horizontal and vertical co-polar returns. Because the peak power of the amplifiers was slightly weak, observations were made with a long pulse to increase the mean power. A pulse compression technique with a linear FM chirp was used to increase range resolution. The range side lobe associated with this technique was suppressed to less than −48 dB (Yamauchi et al. 2012). Because radar cannot observe in the vicinity of the antenna with long-pulse observations, this radar alternately transmitted short and long pulses to cover the blind region associated with the long-pulse observations. The operating frequencies deployed for the two pulses were separated to avoid mutual contamination. The configuration and operating parameters of the radar are summarized in Table 1.

The rotation speed sequence of the antenna shown in Table 1 enables a temporal resolution of volumetric scans with this system of 4 min with 15 elevation observations including the vertical. Vertical measurement in rain was used to calibrate the Z_{DR} measurements to make the uncertainty in the individual range gate Z_{DR} values less than 0.1 dB, as proposed by Illingworth (2004) and Gourley et al. (2009). Beam blocking was common at the lowest elevation angle of 0.5°, so unblocked data at an elevation angle of 1.0° were used in the evaluations below. Because the elevation angle was quite small, the effect of antenna elevation angle on polarimetric measurements is not considered in the evaluations.

3.2 Evaluation of retrieved rainfall rates during the passage of a typhoon

Typhoon Roke passed across the Kanto Plain, on which the MRI is located, in September 2011. Precipitation including heavy rainfalls due to spiral rain bands associated with the typhoon was observed in the Kanto Plain and may have caused significant rain attenuation for the radars operating at C-band or higher frequencies. The MACS-POL radar observations indicate that the center of Roke was located within only 20 km sowtheast of the Kumagaya station at 1820 JST. Rainfall associated with the typhoon continued for about 10 h at the Kumagaya site, which may be long enough for the comparison to provide statistical results and evaluate the reliability of the proposed method. In this comparison, thus, we used the Parsivel optical disdrometer (Löffler-Mang and Joss 2000) measurements at the Kumagaya (KMG) station located about 67.9 km west–northwest of the MRI site, where a weighing (Pluvio^2) precipitation gauge (Nemeth 2008) and an operational tipping-bucket rain gauge were co-located. The time and rain amount resolutions of the

aadachi @mri-jma.go.jp

tipping-bucket rain gauge (Pluvio) were 10 min (1 min) and 0.5 mm (0.03 mm), respectively. The total rainfall amount measured with the Pluvio (84 mm) at the Kumagaya site during the evaluation period agreed well with that measured with the operational rain gauge (87 mm) despite strong winds associated with the typhoon.

Comparisons were made using data recorded from 1000 to 2000 JST on 21 September 2011. The radar-estimated rainfall-rate data available for the single point nearest the Kumagaya station were used for the comparisons. In this evaluation, the range profiles of Z_H and Z_{DR} were smoothed by applying a 1.5-km (= 10-gate) running mean filter before obtaining theoretical ΦDP profiles in order to suppress the standard deviation of the Z_{DR} statistical fluctuations less than 0.2 dB in the running window at most of the range bins. In the retrievals, we found that a value of the shape parameter of 0–2 was best to fit the theoretical Φ_{DP} profiles with those of smoothed-observed Ψ_{DP} in the comparison period. A raindrop temperature of 20 °C was estimated from the surface observations with the dray adiabatic lapse rate and used in the retrievals. The type of precipitation was determined from wind profiler measurements at Kumagaya, which was a part of the Wind profiler Network and Data Acquisition System (WINDAS: Ishihara et al. 2006), by use of the method proposed by Williams et al. (1995).

Time series of (a) rainfall rate, (b) reflectivity, (c) differential reflectivity, (d) median volume diameter derived from the ground measurements and the radar observations at Kumagaya appear in Fig. 3. The thin line in each panel shows the 1-min mean rainfall rate obtained by the surface observations, and the closed circles indicate the radar estimates with the proposed method every 4 min. This figure shows that the radar estimations by the proposed method generally agree well with the surface measurements of both rainfall rate (Fig. 3a) and rain microphysical parameters (Figs. 3b–3f) despite several abrupt variations of rainfall rate and type of precipitation in the time associated with the passage of rain bands of the typhoon. On the contrary, the radar estimates without attenuation correction, indicated by the open

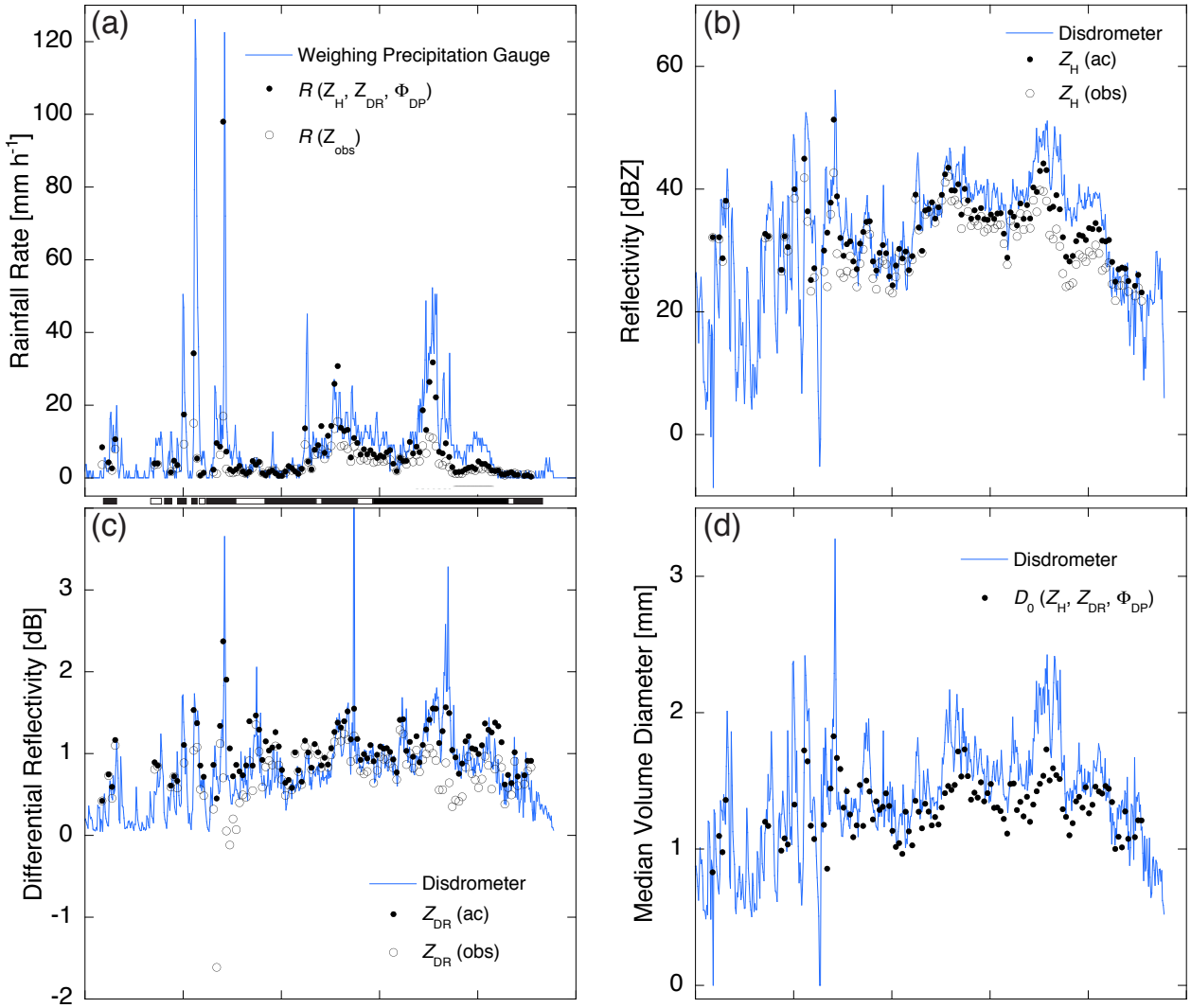

Figure 3. Time series of (a) rainfall rates, (b) horizontal reflectivities, (c) differential reflectivities, (d) median volume diameters, derived from surface measurements (thin line) and estimated from polarimetric radar data (circles) at the Kumataga station from 1000 to 2000 JST on 21 September 2011. The black (white) thick line at the bottom of (a) represents the period of convective (stratiform) rain.

aadachi @mri-jma.go.jp

circles in Figs. 3a–3c, have distinct underestimation tendencies. Indeed, Fig. 3a clearly shows that the proposed method outperforms R(Zobs), particularly in heavy rainfall.

Scatter diagrams comparing the Pluvio rainfall rate with those estimated from the radar observations are shown in Fig. 4. The statistics for the sample rainfall rate shown in Fig. 4 are given in Table 2, along with the corresponding statistics for the data with the classified rainfall rates. In Fig. 4 closed circles and open crosses indicate data from the proposed method and $R(Z_{obs})$, respectively, whereas small (large) open circles represent $R(Z_H, Z_{DR})$ ($R(K_{DP})$). Radar data that did not have corresponding Pluvio data at the same time were removed before the comparison; that is, the same number of observations is used for each method in the figure. In order to compensate for the difference in observational heights (the radar beam center observed precipitation about 900 m above the Kumagaya station), the times of the radar measurements were adjusted to match those of the Pluvio using the empirical terminal velocity (Lhermitte 1990) of the median volume diameter (D_0) of the raindrops estimated with the proposed method.

This figure clearly shows that the three methods with polarimetric measurements, ($R(Z_H, Z_{DR}, \Phi_{DP})$, $R(Z_H, Z_{DR})$, and $R(K_{DP})$), in the retrieval of rainfall rates outperform $R(Z_{obs})$ and are particularly reliable in heavy rain, which is reflected in the linear regressions for the data. The linear regression for the proposed method is close to that of $R(K_{DP})$ and is almost on the 1:1 line, despite the difference in observational space and averaging time between the two measurements, whereas the linear regression for $R(Z_H, Z_{DR})$ indicates a slight tendency to underestimate. In contrast, the linear regression for $R(Z_{obs})$ shows a more than 70% underestimation tendency. These differences are reflected in the statistics for the radar rainfall estimates versus the Pluvio measurements in Table 2.

The statistics for the sample rainfall rates are given in Table 2, along with the corresponding statistics for the data estimated from the radar measurements for different algorithms and thresholds. The rainfall rates measured with the Pluvio are used for the rainfall rate classifications with a threshold value. Note that the minimum detectable rainfall rate with the Pluvio was 1.8 mm h^{-1}, but all the data in the comparison period were considered. However, Pluvio data that

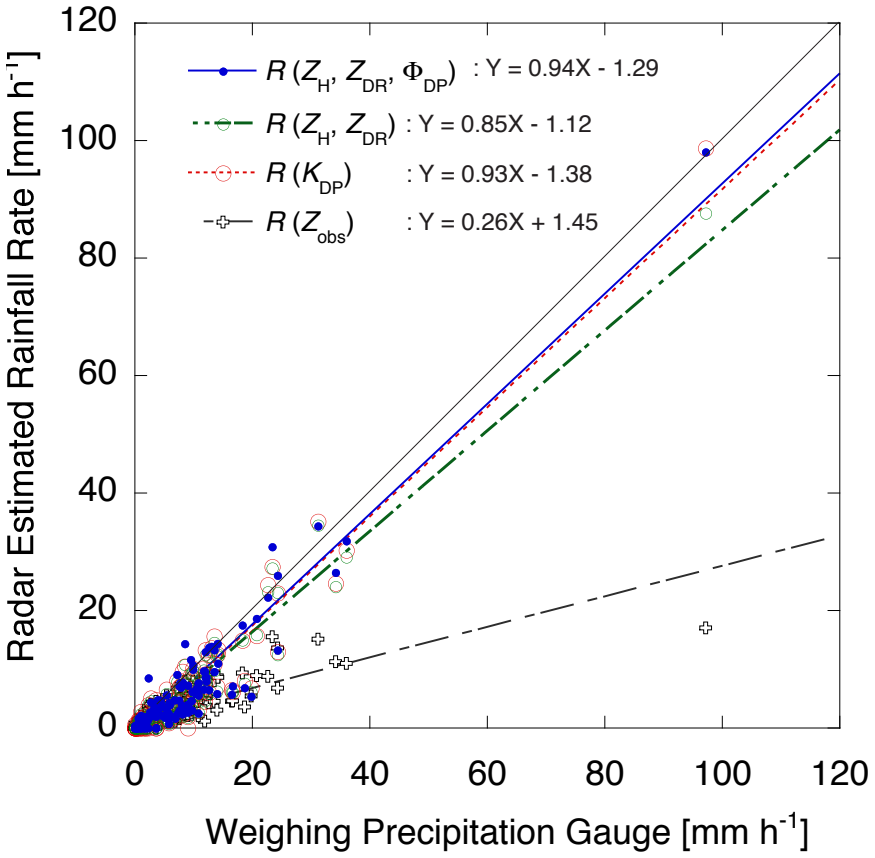

Figure 4. Scatter plot of the rainfall rate measured by the weighing precipitation gauge compared to that estimated from the polarimetric radar data at the Kumagaya station from 1000 to 2000 JST on 21 September 2011. Rainfall rates were estimated using attenuation-corrected Z_H, Z_{DR}, and theoretical Φ_{DP} (closed circles), attenuation-corrected Z_H and Z_{DR} (small open circles), K_{DP} derived from theoretical Φ_{DP} (large open circles) and observed Z_H without attenuation correction (open crosses), respectively. The lines represent linear regressions for each dataset, shown in the upper legend. The thin line is 1:1.

aadachi @mri-jma.go.jp

Table 2. Statistical values for comparison of the radar estimates ($R(Z_H, Z_{DR}, \Phi_{DP})$, $R(Z_H, Z_{DR})$, $R(K_{DP})$ and $R(Z_H)$) vs. Pluvio measurements of the (top row) total points and mean Φ_{DP}, (2nd row) bias, (3rd row) standard deviation, (4th row) root mean square, (5th row) intercept coefficient of the linear regression, (6th row) slope coefficient, and (bottom) correlation coefficient of the rainfall rate differences.

		All Data	$R \geq 2$ mm h^{-1}	$R \geq 5$ mm h^{-1}	$R \geq 10$ mm h^{-1}	$R \geq 15$ mm h^{-1}	$R \geq 20$ mm h^{-1}
Total points		137	90	61	34	14	9
Mean Φ_{DP}		28.3	27.4	32.5	36.8	43.9	49.4
Bias (mm h^{-1})	$R(Z_H, Z_{DR}, \Phi_{DP})$	-1.8	-2.0	-2.8	-3.5	-4.2	-1.4
	$R(Z_H, Z_{DR})$	-2.2	-2.7	-3.6	-4.5	-6.1	-4.1
	$R(K_{DP})$	-1.9	-2.3	-3.1	-3.8	-4.9	-2.4
	$R(Z_H)$	-4.2	-5.7	-7.9	-11.5	-19.1	-22.9
Standard deviation (mm h^{-1})	$R(Z_H, Z_{DR}, \Phi_{DP})$	3.2	3.6	3.9	4.6	6.4	5.3
	$R(Z_H, Z_{DR})$	3.1	3.4	3.7	4.3	5.6	5.6
	$R(K_{DP})$	3.1	3.4	3.8	4.4	5.8	5.4
	$R(Z_H)$	8.0	9.3	10.6	13.0	17.5	20.9
Rms difference (mm h^{-1})	$R(Z_H, Z_{DR}, \Phi_{DP})$	3.6	4.1	4.8	5.7	7.7	5.5
	$R(Z_H, Z_{DR})$	3.8	4.3	5.2	6.3	8.3	6.9
	$R(K_{DP})$	3.6	4.1	4.9	5.8	7.6	5.9
	$R(Z_H)$	9.0	10.9	13.2	17.4	26.0	31.0
Intercept coefficient of the linear regression	$R(Z_H, Z_{DR}, \Phi_{DP})$	-1.29	-1.70	-2.92	-4.34	-6.97	-2.02
	$R(Z_H, Z_{DR})$	-1.12	-1.50	-2.39	-3.34	-5.36	-0.66
	$R(K_{DP})$	-1.38	-1.97	-3.25	-4.66	-8.02	-4.00
	$R(Z_H)$	1.45	2.40	3.38	4.48	5.87	9.13
Slope coefficient of the linear regression	$R(Z_H, Z_{DR}, \Phi_{DP})$	0.94	0.97	1.01	1.05	1.09	1.02
	$R(Z_H, Z_{DR})$	0.85	0.88	0.91	0.94	0.97	0.90
	$R(K_{DP})$	0.93	0.96	1.01	1.05	1.11	1.05
	$R(Z_H)$	0.26	0.23	0.19	0.16	0.13	0.08
Correlation coefficient	$R(Z_H, Z_{DR}, \Phi_{DP})$	0.95	0.95	0.96	0.96	0.96	0.97
	$R(Z_H, Z_{DR})$	0.96	0.96	0.96	0.96	0.96	0.97
	$R(K_{DP})$	0.96	0.96	0.96	0.97	0.97	0.98
	$R(Z_H)$	0.79	0.75	0.70	0.66	0.62	0.57

did not have corresponding radar data for the same time were removed before the comparison.

All the statistical data show that $R(Z_H)$ has the lowest reliability of the four rainfall retrieval algorithms as expected. It has the worst bias, standard deviation, root mean square, and coefficients of liner regression and correlation among the methods. The statistical data for $R(Z_H)$ became worse with the threshold of rainfall rate. This is likely because the effect of attenuation by precipitation became large with rainfall rate, which is supported by an increase of mean Φ_{DP} with the threshold of rainfall rate. On the other hand, slope coefficients and correlation coefficients for the three methods with polarimetric measurements are close to unity and almost independent of the threshold of rainfall rate, although the slope coefficient for $R(Z_H, Z_{DR})$ indicates a slight tendency to underestimate.

Both the standard deviation and root mean square difference of the three methods with polarimetric measurements tend to increase with the threshold of the rainfall rate. The reason for these increases may include the decrease in sample number with rainfall rate. The standard deviations for these methods in the same threshold of rainfall rate are very similar. However, the rainfall rates with the proposed method and $R(K_{DP})$ always have smaller bias and root mean square of difference than $R(Z_H, Z_{DR})$, which may reflect the characteristics of the slope coefficients.

4. Conclusions

We developed an algorithm for rain attenuation correction of the reflectivity factor and differential reflectivity measured by polarimetric radar at attenuating frequency to retrieve DSD parameters and rainfall rate. The algorithm presented in this study was developed based on the self-consistency principle, describing the interrelation between polarimetric measurements along the range profile. It does not require any assumptions of relationship among DSD parameters and/or simplifications of relationship between the axis ratio and diameter of raindrops, which were used in previous studies. Moreover, the proposed algorithm needs no external reference data such as 2DVD measurements for attenuation corrections because it retrieves the co-polar and differential specific attenuations from interrelation among the polarimetric measurements. Additionally, the algorithm retrieves three parameters of the modified gamma distribution, from which rain parameters including rainfall rate can be theoretically estimated.

The performance of this algorithm was evaluated by comparison with optical disdrometers and a weighing precipitation gauge. The evaluation of the algorithm showed fairly good agreement between the retrieved median volume diameter of raindrops and both reflectivity and differential reflectivity with those obtained by surface measurements irrespective of convective and stratiform precipitation conditions. Additionally, the algorithm

aadachi @mri-jma.go.jp

demonstrated significant improvement in performance for rainfall rate estimation compared with rates estimated using the so-called *Z–R* relationship. Results also showed that the algorithm has comparable accuracy and precision of rainfall rate with those estimated from specific differential phase.

It is noteworthy that this algorithm is available for only pure rain. Contamination by ice hydrometeors, including hail and/or graupel, irrespective of dry or wet conditions along a rain path in a radial direction, may result in large errors in the retrievals of rain parameters with the proposed algorithm. However, contamination other than that from pure rain including ground clutters and/or partial beam blockage in a radial direction can be identified and discarded by this method because it causes a large discrepancy of the theoretical Φ_{DP} profile from the smoothed-observed Ψ_{DP}. Ice hydrometeors can also be detected to some extent from polarimetric measurements (e.g., Golestani et al. 1989; Park et al. 2009; Cifelli et al. 2011; Adachi et al. 2013a). In this case, $R(K_{DP})$ can be used for estimation of rainfall rates as long as ice hydrometeors are dry (e.g., Picca and Ryzhkov 2011; Ryzhkov et al. 2009), although DSD parameters cannot be deduced with the method.

Acknowledgements

The authors express appreciation to Dr. M. Thurai of Colorado State University for many helpful discussions and comments regarding the research presented. We also express our appreciation to Prof. A. Illingworth of the University Reading for his valuable input and guidance on the auto-calibration technique. The first author thanks S. Onogi of MRI for offering source codes for WINDAS data. This study was partially supported by the funds for integrated promotion of social system reform, research, and development of the Ministry of Education, Culture, Sports, Science and Technology (MEXT) of Japan.

References

Adachi A, Kobayashi T, Yamauchi H, Onogi S. 2013a. Detection of potentially hazardous convective clouds with a dual-polarized C-band radar. Atmos. Meas. Tech. : Vol. 6, 2741-2760. DOI: 10.5194/amt-6-2741-2013.

Adachi A, Kobayashi T, Yamauchi H, Onogi S. 2013b. Radar calibration using polarimetric observations with rain attenuation correction. In Proceedings of 36th Conference on Radar Meteorology. Breckenridge, CO, Amer. Meteor. Soc., P270.

Brandes EA, Zhang G, Vivekanandan J. 2005. Corrigendum. J. Appl. Meteor. : Vol. 44. 186-186.

Bringi VN, Thurai M, Nakagawa K, Huang GJ, Kobayashi T, Adachi A, Hanado H, Sekizawa S. 2006. Rainfall estimation from C-band polarimetric radar in Okinawa, Japan: Comparison with 2D-video disdrometer and 400 MHz wind profiler. J. Meteor. Soc. Japan. : Vol. 84, 705-724.

Cifelli R, Chandrasekar V, Lim S, Kennedy PC, Wang Y, Rutledge SA. 2011. A new dual-polarization radar rainfall algorithm: Application in Colorado precipitation events. J. Atmos. Oceanic Technol. : Vol. 28, 352-364.

Goddard JWF, Tan J, Thurai M. 1994. Technique for calibration of meteorological radars using differential phase. Electron. Lett. : Vol. 30, 166-167.

Golestani Y, Chandrasekar V, Bringi VN. 1989. Intercomparison of multiparameter radar measurements. Preprints of 24th Conf. on radar meteorology. Amer. Meteor. Soc., Tallahassee, Florida, 309-314.

Gorgucci E, Bechini R, Baldini L, Cremonini R, Chandrasekar V. 2013. The influence of antenna radome on weather radar calibration and its real-time assessment. J. Atmos. Oceanic Technol. : Vol. 30, 676-689.

Gorgucci E, Scarchilli G, Chandrasekar V. 1992. Calibration of radars using polarimetric techniques. IEEE Geoscience Remote Sencs. 30: 853-858. DOI: 10.1109/36.175319.

Gourley JJ, Illingworth AJ, Tabary P. 2009. Absolute calibration of radar reflectivity using redundancy of the polarization observations and implied constraints on drop shapes. J. Atmos. Oceanic Technol. : Vol. 26, 689-703.

Illingworth AJ. 2004. Improved precipitation rates and data quality by using polarimetric measurements. In: Meischner, P. (ed.) Weather radar: Principles and advanced applications. Springer-Verlag, Berlin, 130-166.

Ishihara M, Kato Y, Abo T, Kobayashi K, Izumikawa Y. 2006. Characteristics and performance of the operational wind profiler network of the Japan Meteorological Agency. J. Meteor. Soc. Japan. : Vol. 84, 1085-1096.

Le Bouar E, Testud J, Keenan TD. 2001. Validation of the rain profiling algorithm "ZPHI" from the C-band polarimetric weather radar in Darwin. J. Atmos. Oceanic Technol. : Vol. 18, 1819-1837.

Lhermitte R. 1990. Attenuation and scattering of millimeter wavelength radiation by clouds and precipitation. J. Atmos. Oceanic Technol. : Vol. 7, 464-479.

Löffler-Mang M, Joss J. 2000. An optical disdrometer for measuring size and velocity of hydrometeors. J. Atmos.

 aadachi @mri-jma.go.jp

Oceanic Technol. : Vol. 17, 130-139.

Nemeth K. 2008. OTT Pluvio²: Weighing precipitation gauge and advances in precipitation measurement technology. TECO-2008 - WMO Technical Conference on Meteorological and Environmental Instruments and Methods of Observation (TECO-2008), St. Petersburg, Russian Federation.

Park, H. S., A. V. Ryzhkov, D. S. Zrnić, and K.-E. Kim, 2009: The hydrometeor classification algorithm for the polarimetric WSR-88D: Description and application to an MCS. Wea. Forecasting. : Vol. 24, 730-748.

Picca J, Ryzhkov A. 2011. A dual-wavelength polarimetric analysis of the 16 May 2010 Oklahoma city extreme hailstorm. Mon. Wea. Rev. : Vol. 140, 1385-1403.

Ryzhkov AV, Giangrande S, Khain A, Pinsky M, Pokrovsky A. 2009. `Polarimetric characteristics of melting hail at S and C bands`. In Proceedings of 34th Conference on Radar Meteorology. Williamsburg, VA, , Amer. Meteor. Soc., 4A.6.

Testud J, Le Bouar E, Obligis E, Ali-Mehenni M. 2000. The rain profiling algorithm applied to polarimetric weather radar. J. Atmos. Oceanic Technol. : Vol. 17, 332-356.

Thurai M, Hanado H. 2005. Absolute calibration of C-band weather radars using differential propagation phase in rain. Electronics Letters. : Vol. 41, 1405-1406.

Ulbrich CW. 1983. Natural variations in the analytical form of the raindrop size distribution. J. Climate Appl. Meteor. : Vol. 22, 1764-1775.

Williams CR, Ecklund WL, Gage KS. 1995. Classification of precipitating clouds in the tropics using 915-MHz wind profilers. J. Atmos. Oceanic Technol. : Vol. 12, 996-1012.

Yamauchi H, Adachi A, Suzuki O, Kobayashi T. 2012. `Precipitation estimate of a heavy rain event using a C-band solid-state polarimetric radar`. In proceedings of 7th European Conference on Radar in Meteorology and Hydrology, Toulouse, France 24-29 June 2012. Météo France: Toulouse.

Yoshikawa E, Chandrasekar V, Ushio T. 2014. Raindrop size distribution (DSD) retrieval for X-band dual-polarization radar. J. Atmos. Oceanic Technol. : Vol. 31, 387-403.

aadachi @mri-jma.go.jp